Available online at www.sciencedirect.com

jmr&t Journal of Materials Research and Technology

www.jmrt.com.br

Original Article

Titanium carbide coating on graphene nanoplatelets

Mahmood Khan[a,b,*], Salman Ahmad[b], Sarim Zaidi[b], Abdul Wadood[b], Tayyab Subhani[c], Shahid Akhtar[d], Syed Wilayat Husain[b], Ragnhild Elizabeth Aune[a]

[a] Department of Materials Science and Engineering, Faculty of Natural Sciences, Norwegian University of Science and Technology, 7491 Trondheim, Norway

[b] Department of Materials Science and Engineering, Institute of Space Technology, Islamabad, 44000, Pakistan

[c] Department of Mechanical Engineering, College of Engineering, University of Hail, Ha'il, Saudi Arabia

[d] Norsk Hydro, Karmøy Primary Production, Hydrovegen, N-4265 Håvik, Norway

ARTICLE INFO

Article history:
Received 11 December 2018
Accepted 13 January 2020
Available online 24 January 2020

Keywords:
Titanium carbide
Graphene nanoplatelets
Aluminium
Composite
Coating

ABSTRACT

Titanium carbide was formed on graphene nanoplatelets (GNPs) using potassium hexafluorotitanate (K_2TiF_6) salt in the presence of pure aluminium. K_2TiF_6 - GNPs mixture with titanium to carbon ratio of 5:1 was heated at a high temperature of 900 °C for 1 h under argon atmosphere. Energy dispersive spectroscopy indicated the presence of elemental titanium on the surface of GNPs, while the presence of titanium carbide was verified by X-ray diffraction. Scanning electron microscopy confirmed the morphology of titanium carbide-coated nanoplatelets embedded in aluminium melt. Thermal characterisation was carried out by differential scanning calorimetry to identify the reaction kinetics and products of the reactions. This facile process to coat titanium carbide on GNPs offers a possibility to reduce the wettability issues of GNPs in the aluminium matrix and enhance the dispersion with an opportunity to prepare hybrid aluminium matrix composites. The present study deals with in-situ synthesis of titanium carbide on GNPs, which aims to prepare nano-reinforced hybrid reinforcement aluminium matrix composite.

1. Introduction

Aluminium matrix composites containing graphene nanoplatelets (Al-GNPs) are gaining considerable attention due to their improved properties as desired in the aerospace and automobile industries [1,2]. However, the inert nature of carbon presents wetting problems in metal matrix composites (MMCs). The situation aggravates when referring to nano reinforcements of carbon, such as carbon nanotubes (CNTs) [3,4] and graphene nanoplatelets (GNPs) [5,6]. The dispersion problems of CNTs and GNPs arises along with wetting issues due to significant difference in surface tension forces, i.e., 45 mN/m (carbon) and 955 mN/m (aluminium) [7].

The superior mechanical and functional properties of GNPs make them an ideal choice for reinforcement in MMCs. Few of these are; 1 TPa modulus of elasticity, 125 GPa fracture strength, 5000 W m^{-1} K^{-1} thermal conductivity and 200,000 cm^2 V^{-1} s^{-1} carrier mobility [8,9]. The ideal situation

* Corresponding author.
E-mail: mahmood.khan@ntnu.no (M. Khan).

https://doi.org/10.1016/j.jmrt.2020.01.053

wherein GNPs may provide optimum advantages in MMCs is their homogeneous distribution, together with the absence of unwanted interfacial reactions with the matrix material. In the case of aluminium, the formation of aluminium carbide (Al_4C_3) reduces the overall composite properties due to the fragile nature of interfacial carbide coupled with its poor corrosion resistance [10]. Moreover, the presence of a thin aluminium oxide (Al_2O_3) layer on the surface of aluminium particles (as matrix material) restricts the sintering of the composite. This issue is addressed by sintering in inert environments like argon or nitrogen [2]. The presence of an oxide layer on aluminium powders can also lead to a problem related to the intimate contact with GNPs, resulting in failure of bonding with the matrix and poor mechanical properties of Al-GNPs composites.

Indeed a desirable and stable interface improves the strength of the composites by transferring the applied load from matrix to reinforcement. As a result, different metals have been investigated as the coating material for GNPs. In a study by Q. H. Hu et al., nickel was coated by electroless plating [12] while electrodeposition was employed by C. Liu et al. [13]. The electrodeposition on carbonaceous nano reinforcements is a complicated process compared to metallic substrates. It generally involves two steps: decorating the nano reinforcements with aluminium nanoparticles followed by the addition of aluminium powder on carbonaceous nano reinforcements; still the final step is high-temperature annealing to achieve complete wetting. In-situ processing of nano reinforcement is another option leading to benefits over ex-situ processing. Among these benefits, one is the smaller reinforcement's size and higher surface area, which contributes to higher strength in the resulting multiphase composite [14]. The composites fabricated via in-situ route have clean, unoxidized particle-matrix interfaces with higher interfacial strength and improved wettability [15]. Thermodynamically stable phases are formed and further reaction of decomposition is generally ruled out [16]. The in-situ reinforcing phase is uniformly distributed in the composite matrix [17]. The concept of solubility, as reported by Rana et al. [18–20], can be applied to the present research in a way to designate aluminium as a solution containing solute as GNPs and titanium. The solubility of titanium at 900 °C is around ~22 % [21]. This supports the presence of elemental titanium in the aluminium melt to be available for reaction with GNPs. Contrary to titanium solubility, the presence of GNPs as a stable insoluble [22] site for titanium is strong reason for the formation of titanium carbide (TiC) on GNPs.

Carbonaceous reinforcement, along with alumina in aluminium alloy matrix, has been used for cylinder liners in high-rpm, high power motorcycle engines. Similarly, nickel-coated graphite particles combined with silicon-carbide particles in the aluminium matrix has been used for cylinder liners, cast rotors, and disc brake system [23,24]. The excellent wear behaviour is exhibited by the combination of solid-state lubrication of graphite and high-temperature strengthening of the matrix alloy [23]. Nano hybrid reinforcement for aluminium matrix composites has been reported to possess the strength advantage over conventional composites because the Orowan strengthening effect is greatly enhanced [25]. Nano sized reinforcements are also favourable for the grain boundary pinning; hence they result in smaller matrix grain size. Therefore, the final composite exhibits an improvement in strength and other mechanical properties [26]. TiC is, thermally, a very stable refractory metal carbide and possesses high hardness. In a study, efforts were made to fabricate TiC/Al composites using in-situ methods [27]. In in-situ TiC/Al composites, however, TiC particles often exist in clusters, and it is challenging to disintegrate these TiC clusters. The hybridisation of different types of reinforcements is attractive because this approach can be used to tailor the properties of the composites [28]. The hybridisation of carbonaceous nano reinforcement with TiC results in lower content to be added in the matrix and improved distribution [29]. Hybrid reinforced aluminium matrix composites are generally used for electrical sliding contact, tire stud, drive shaft in Chevrolet S-10 [30].

The present work presents a novel approach to address the problem of dispersion and wetting issues of GNPs in the aluminium matrix by in-situ formation of TiC on GNPs in aluminium melt. A facile approach to address the wetting and dispersion issues to coat GNPs with TiC from potassium hexafluorotitanate (K_2TiF_6) salt is presented in this study. The use of K_2TiF_6 salt as flux offers the following advantages: (a) it has the capability to dissolve Al_2O_3 layer and prevents further oxidation, (b) it provides active site by decomposition and coating of reinforcements [31] and (c) it acts as precursor of titanium, which can be electrolessly coated on the surface of carbonaceous reinforcements [32]. The developed coating was characterised for microstructure and morphology by scanning electron microscopy (SEM), energy dispersive spectroscopy (EDS), and X-ray diffraction (XRD) while reaction kinetics were studied by differential scanning calorimetry (DSC).

2. Experimental

Fig. 1 shows scanning electron microscopic (SEM) images of raw materials; GNPs were purchased from Guangzhou Jiechunang Trading Co. Ltd. China with 2–5 μm diameter and ~10 nm thickness (Fig. 1a) while 99.6 % pure aluminium flakes of particle size 50 μm were used (Fig. 1b); K_2TiF_6 (Fig. 1c) was used and the flux with purity > 99 %, was supplied by Sigma-Aldrich, USA.

A novel approach was opted to prepare the powder by mixing 2.5 g of aluminium flakes, 2.5 g of K_2TiF_6 salt and 0.1 g of GNPs (with Ti to C ratio of 5:1) and milling in a ball mill (Model No RZ-04149-05, Cole-Parmer Instrument Company, LLC., United States) at 100 rpm for 15 min. The purpose of mixing was to ensure the proper distribution of GNPs, aluminium flakes and salt so that the maximum contact among the constituent materials can be established during subsequent heating. The mixture was transferred into a porcelain crucible and placed in a tube furnace (Model no. KJ-1600VF, Kejia Furnace Co. Ltd. China) and heated to 900 °C in an argon atmosphere. The heating rate of 5 °C/min was applied to the targeted temperature with the holding time of one hour, followed by furnace cooling. The heated mixture was ground in a mortar with pestle followed by filtration in a buffer solution of distilled water for separating undesirable residue from the heated mixture. Fig. 2 shows the schematics of the complete process.

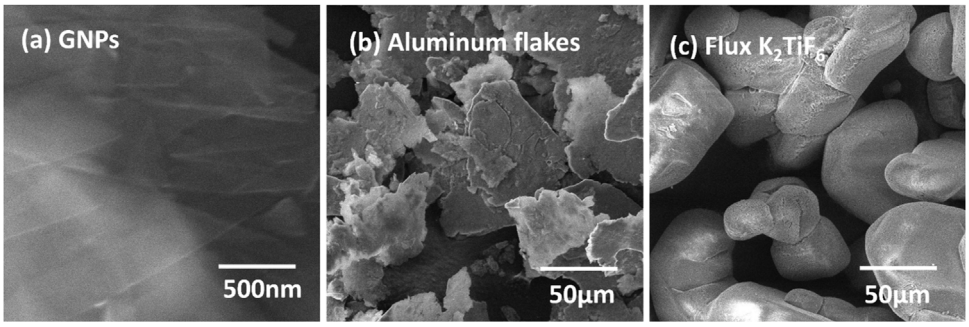

Fig. 1 – SEM images of raw materials: (a) GNPs, (b) aluminium flakes, (c) K_2TiF_6 salt.

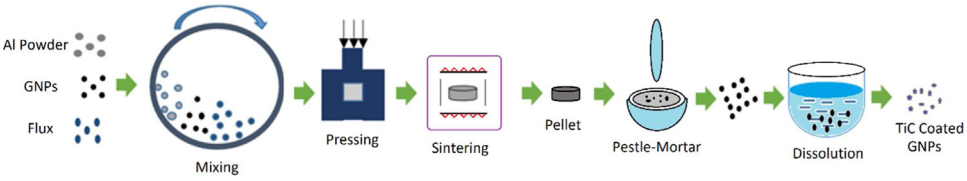

Fig. 2 – Schematics of the process carried out to coat the GNPs with TiC.

For microstructural characterisation, the purified heated mixture was observed under SEM in secondary electron imaging mode at 20 kV accelerating potential. EDS was performed on a spectrometer (X-MaxN Silicon Drift Detector, Oxford Instruments, UK) attached to the SEM microscope. To evaluate various reactions in the mixture at different temperatures, DSC was carried out on constituent materials and the mixture. For this purpose, 10 mg of the mixture was heated to 800 °C in argon in the DSC (NETZSCH STA 409C Gerätebau GmbH, Germany) setup. A heating rate of 10 °C/min and a constant flow of argon were maintained throughout the heating cycle. The heated mixture was characterised for phase analysis in XRD (GNR instruments analytical group, Italy) using an X-ray source with CuK_α radiation having a wavelength of 1.54 Å. The diffractometer was operated at 40 kV and 30 mA tube potential and current respectively with a scan rate of 0.1° per minute and a step size of 0.05° in 2 theta range of 20 to 80°.

3. Results and discussion

3.1. EDX

Fig. 3a–c show the SEM images of filtered TiC coated GNPs with characteristic morphological appearance of graphene sheets. Fig. 3d and e show EDS of TiC coated GNPs and filtered out mass of potassium fluoroaluminate ($KAlF_4$). Elemental distribution of five elements, i.e., carbon, titanium, aluminium, potassium and fluorine various drastically in filtered and filtered out mass. The existence of these elements confirms the hypothesis of the formation of TiC covered GNPs with a trace amount of unfiltered impurities. The EDS of filtered out mass clearly shows the residue of salt decomposition (Fig. 3e). The presence and comparatively excessive amount of titanium and carbon suggested the existence of TiC [33]. Indeed, as heating the GNP/aluminium/salt mixture at 900 °C, is expected to form TiC at preferential sites of GNPs under aluminium melt. The only source of carbon in the raw materials is GNPs. The active carbon sites for reaction with titanium are the defective/missing carbon atoms on GNPs sheet/surface. Possibly due to the existence of a mixture of TiC and GNPs (as carbon source) and the formation of TiC on GNPs is further explored by the XRD examination.

3.2. XRD

Fig. 4 shows the XRD patterns of constituent materials along with the heated mixture. The individual constituents, K_2TiF_6 salt and aluminium showed typical peaks corresponding to the positions reported by Rodriguez et al. [34] and Khan et al. [1,35], respectively. The heated mass is densified due to aluminium melting and its solidification. High temperature aided the floatation of residue at the top and easy removal through water filtration. Still the traces of potassium fluoroaluminate ($KAlF_4$) were identified, as indicated in elemental analysis in Fig. 3e. The presence of $KAlF_4$ caused the removal of potassium and titanium oxides [36]. The peak representing GNPs is at 25° [37], while the peaks corresponding to salt diminished in the filtered mass. TiC and partially converted titanium dicarbide (TiC_2) peaks were observed at specific positions in agreement with earlier studies [38]. TiC peaks were found at 35.5, 41.8, and 59.8° along with Al_3Ti peak at 24.9° as reported by Birol [36] at similar positions of 2 theta. The possible existence of Ti-Al-C can be ruled out based on present XRD results and the investigation of Wang et al. [39]. Peaks of $KAlF_4$ and K_3AlF_6 were found at their specific locations of 28.7, 36.2 and 29.8°, respectively [33]. EDS also confirm the elemental presence of potassium as these salts aid titanium to react with carbon, which is present in the form of GNPs and early melting of aluminium. The presence of potassium fluoride (KF) in XRD is superimposed on the same 2 theta angle as TiC, i.e.41.7° [40]. The DTA shows an exothermic rise in Fig. 6, which pertains to

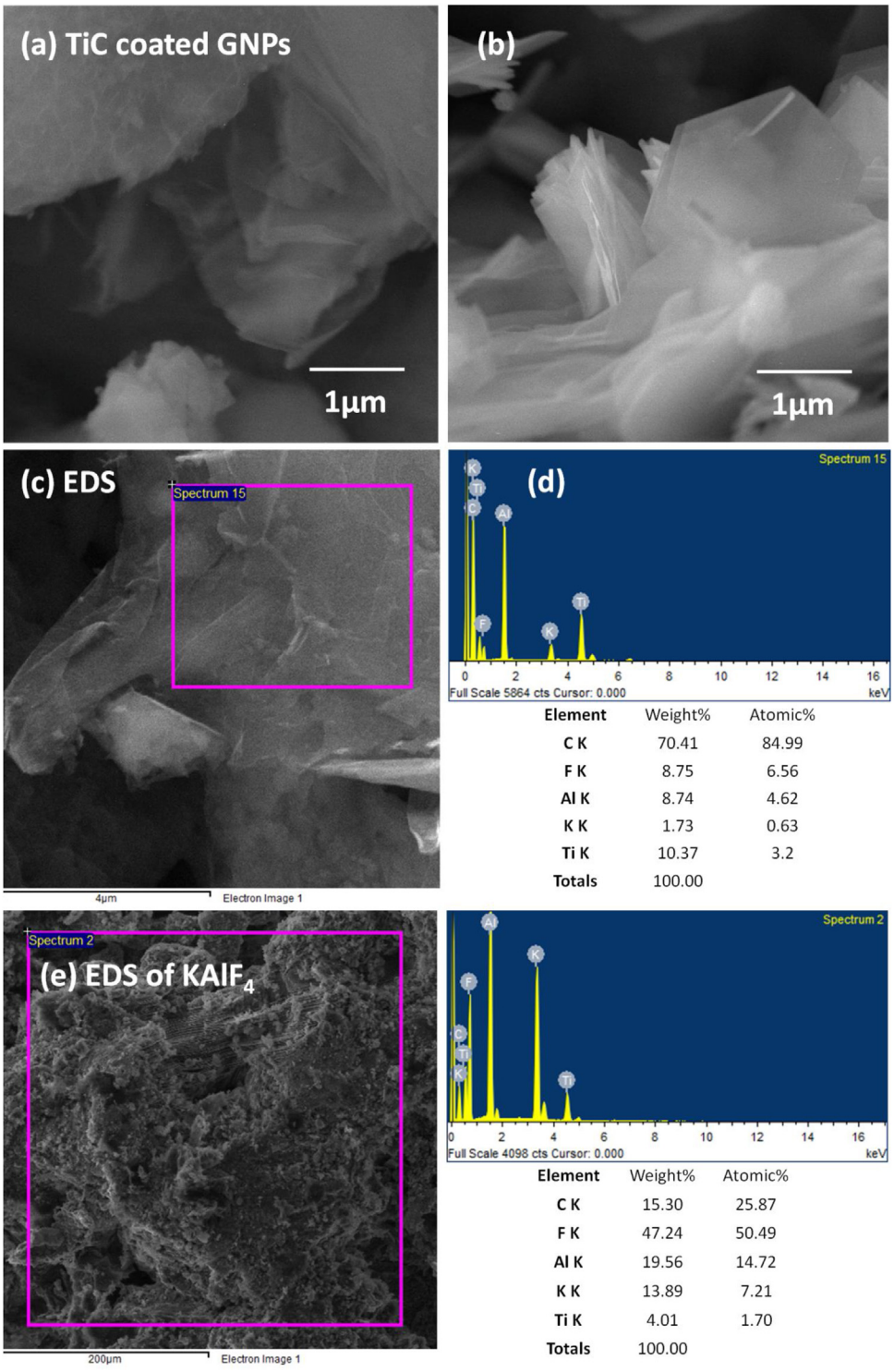

Fig. 3 – SEM images of; a), b) and c) titanium carbide coated GNPs, d) EDS results showing the presence of titanium and carbon and (e) EDS of $KAlF_4$.

the formation of TiC. The presence of Al_3Ti is due to the reaction of K_2TiF_6 with molten aluminium. This results in release of titanium, which dissolves in the aluminium melt. When the solubility limit of titanium in liquid aluminium at the reaction temperature is exceeded, $TiAl_3$ precipitates according to the Al- Ti phase diagram [41].

3.3. *DTA*

DTA spectra of the mixtures and individual constituents are shown in Fig. 5. The spectrum of GNPs (Curve 1) shows shallow endothermic reactions ranging in a temperature range from 480 to 545 °C and an exothermic signal at 680 °C. The

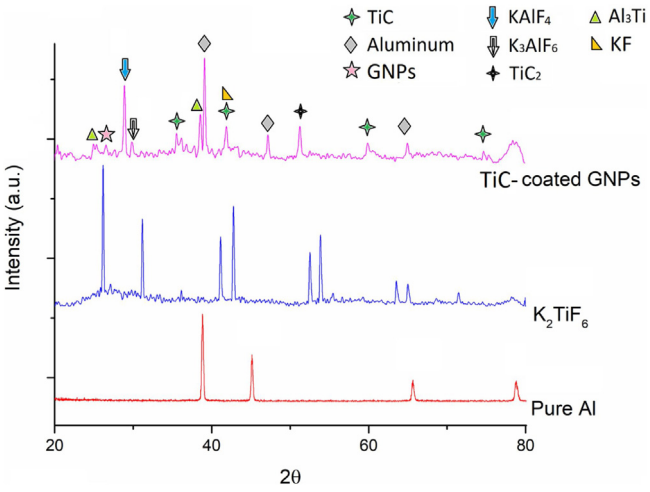

Fig. 4 – XRD data presented as a graph, showing raw materials and heated mixture phases.

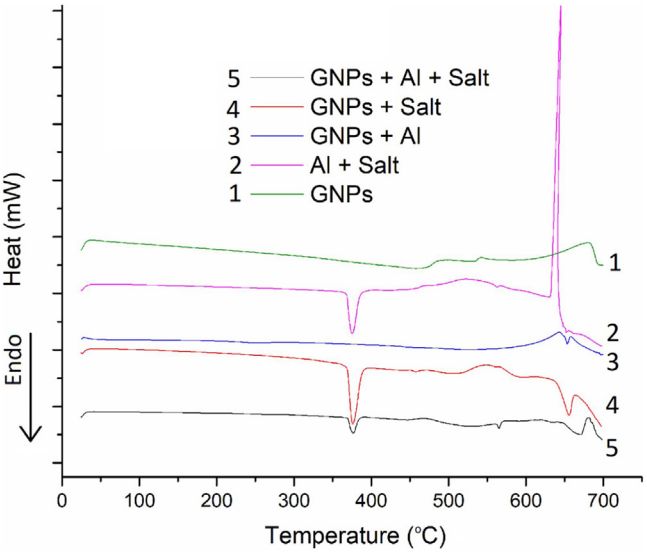

Fig. 5 – Graphs showing DTA of raw materials and filtered mixture containing TiC coated GNPs.

two endothermic humps may be related to the weight-loss due to the removal of moisture and associated residue mass in GNPs. The high-temperature exothermic peak relates to the decomposition of GNPs. The second spectrum (Curve 2) corresponds to the mixture of aluminium and salt. In this curve, the first endothermic peak at 375 °C is associated with the decomposition of salt [34] and indicates that no reaction between aluminium and salt occurred until this temperature. A range of exothermic reactions from 460 to 630 °C can be viewed as the formation of new phases. These can be related to the dissociation of fluoride salt and the release of elemental titanium, as per Eq. (1). A strong exothermic peak at 645 °C is related to the complete reduction of K_2TiF_6 with aluminium and formation of Al_3Ti before the melting of aluminium [42], as shown by Eqs. (2) and (3). The presence of Al_3Ti phase has been confirmed in XRD (Fig. 4) as also verified elsewhere [43]. The endothermic dip in the spectrum at 650 °C is associated with the melting of aluminium, which is lowered due to the presence of salt [32]. The activation temperature for K_2TiF_6 salt is >460 °C, where it starts reacting with aluminium for the formation of the Al_3Ti phase in the binary blend. An earlier study by Prasad et al. [43] reports the temperature of ~700 °C as maximum for the production of Al-Ti master alloy at a specific higher rate of heating compared to as used in the present investigation. However, the minimum temperature for the start of the reaction, Equation (2), was predicted by the same study to be lower. Herein this study, the start of the reaction is found to be around 460 °C.

$$K_2TiF_6 + 4Al \rightarrow 3Ti + 3KAlF_4 + K_3AlF_6 \quad (1)$$

$$Ti + 3Al \rightarrow Al_3Ti \quad (2)$$

$$K_2TiF_6 + 13Al \rightarrow 3Al_3Ti + 3KAlF_4 + K_3AlF_6 \quad (3)$$

The third spectrum (Curve 3) corresponds to the mixture of aluminium with GNPs. The first exothermic peak at 643 °C and the second at 658 °C may correspond to the formation of aluminium carbide (Al_4C_3) [44], which is near the melting endothermic signal of aluminium at 655 °C. The two temperatures are related to starting temperature (643 °C) of formation

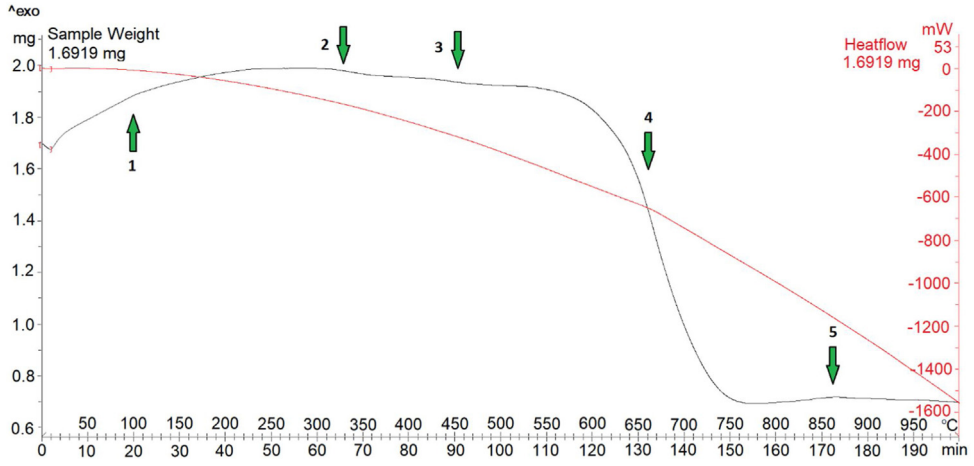

Fig. 6 – Graphs showing the TGA curve coupled with DSC of aluminium, salt and GNPs mixture in equal proportions.

of Al_4C_3 in solid-state and near melting temperature at 658 °C in partially molten state [45]. The formation of Al_4C_3 has suppressed the strong aluminium melting peak, as can be seen in Curve 2 (Al + Salt). The surface area of the melt increases as the density of Titanium and initially formed TiC is higher than aluminium. Eq. (4) shows the reaction:

$$Al + 3C \rightarrow Al_4C_3 \quad (4)$$

The spectrum (Curve 4) of the mixture of GNPs and salt shows the characteristic endothermic peak of salt decomposition at 376 °C [46] while small peaks at 457 and 545 °C correspond to the moisture and associated residue mass removal from GNPs, as also observed in curve 1. The second sharp endothermic peak at 663 °C may represent the start of the formation of TiC, which is expected to develop on the surface of GNPs [38] as the only source of carbon in the raw materials is GNPs. All the three temperatures of the GNPs relate to the DTA curve 1, but the presence of salt has lowered the intensity of ΔH. The dissociation of salts can be attributed to the reduced intensities of ΔH and formation of TiC, as per Eq.s (5) and (7) [47]. Eq. (6) is an equilibrium state of TiF_4 with elemental titanium depending on molar concentration, which eventually results in the formation of TiC as titanium element is consumed and TiF_4 dissociate into titanium.

$$K_2TiF_6 \rightarrow 2KF + TiF_4 \quad (5)$$

$$TiF_n(n = 3, 2, 1) \Leftrightarrow (4-n)Ti + nTiF_4 \quad (6)$$

$$Ti + C \rightarrow TiC \quad (7)$$

In a study by Y. Birol [36], K_2TiF_6 salt and graphite were reacted for the in situ formation of TiC from halide salts. The salt decomposition was carried out by displacement reaction. The third peak at 663 °C provides strong evidence of in situ formation of two carbides of titanium, i.e., TiC and TiC_2 on the surface of GNPs, as also observed in XRD (Fig. 4) [33]. TiF_4 has a melting point of 377 °C and sublimes in the gaseous state.

$$K_2TiF_6 + 2C \rightarrow TiC + 2KF + CF_4 \quad (8)$$

$$Ti + CF_4 \rightarrow TiC + TiF_4 \quad (9)$$

The fifth spectrum (Curve 5) of the mixture containing aluminium, salt and GNPs shows four distinct endothermic reactions that occurred at 376, 447, 565 and 660 °C and three exothermic reactions at 620, 640 and 681 °C. As already discussed, the low-temperature exothermic reaction at 376 °C is associated with salt dissociation. The shallowness in intensity is due to the lower weight fraction used in the tri-constituent mixture, as compared to binary loading curves 2 and 4. The shallow hump at 447 °C represents the formation of new products, as per Eq. (2). Another pertinent salt peak at 565 °C was recorded in all spectra of K_2TiF_6. This is related to the melting of alumino-fluorites salts $KAlF_4$ and K_3AlF_6 formed as per Eqs. (1) and (3). The last and high-temperature peak at 660 °C represents the melting of aluminium, which was not lowered in temperature as in a binary mixture of aluminium and salt. The reason is the higher quantities of reaction products and lower proportion of salt, which lowers the melting point of aluminium. The exothermic reactions at higher temperatures: 620, 640 and 681 °C are related to the formation of TiC on active and available sites of carbon in GNPs, as per Eqs. (2), (7), (10) and (11):

$$C + Al_3Ti \rightarrow 3TiC + Al \quad (10)$$

$$C + 4TiF_4 \rightarrow 3TiF_4 + TiC \quad (11)$$

3.4. TGA

Fig. 6 shows the TGA coupled DSC curve of the mixture containing aluminium, salt and GNPs. In general, the heat flow trend is endothermic due to the melting of aluminium, which absorbs the maximum heat input. The TGA result of this mixture showed a weight loss of about ~60 % up to 1000 °C. The initial marginal mass gain of the mixture sample is associated with the buoyancy effect of the purging gas. A lower mixture mass of 1.691 mg was used. This lower mass was chosen, based on the strong exothermic peak observed in Fig. 5, curve 2. The formation of TiC is an exothermic reaction. Therefore to avoid damage to the alumina crucible and instrument, a lower mass was selected. This lower mass has been affected initially by the gaseous flow and moisture removal and becomes stable at 300 °C (Point 2). The general trend of moisture removal takes place from 100 to 200 °C and salt decomposition starts at ~460 °C (Point 3). It can be seen that the sudden mass loss of the mixture only begins after the first endotherm at ~640 °C. This corresponds to the beginning of aluminium melting, which starts with the formation of Al_3Ti at the surface of aluminium near complete melting at 660 °C (Point 4) [42]. The weight loss of the salt increased with increasing temperature and reached about 60 % of initial mass with dissociation of the salt as per earlier discussed Eq. (5), which conforms with the DTA results. The titanium as metal does not show any mass loss during this treatment [43] due to higher density and thermally stable state. However, the fluorine content of the salt increases as the temperature is raised. The maximum of the mass loss has occurred until this point of aluminium melt, as most of the gaseous elements have been removed and mainly, the solid mass of aluminium with TiC on GNPs sustains with trace impurities. A shallow hump of exothermic at 870 °C (Point 5) appears in TGA (Fig. 6). This hump was not achievable in DSC due to instrument temperature limitation (Fig. 5) and can only be noticed in TGA. This is associated with the formation of TiC as per Eq. (7) in the aluminium melt, as reported by B. Dikici et al. [48].

3.5. TEM

Fig. 7 shows TEM images of TiC coated GNPs with Selected area diffraction (SAD) patterns specific to GNPS and TiC. Fig. 7a shows GNPs (identified by a green box) covered with in-situ TiC nanoparticles. The verification of GNPs was carried out by SAD, which revealed typical 002 and 004 rings of GNPs [49]. Traces of impurities and subsequent TEM sample preparation method is a possible source of masking typical GNPs SAD pattern. Fig. 7a shows ring diffraction patterns pertaining to TiC [50]. The ring patterns are characteristic of nanoparticles typically grown on

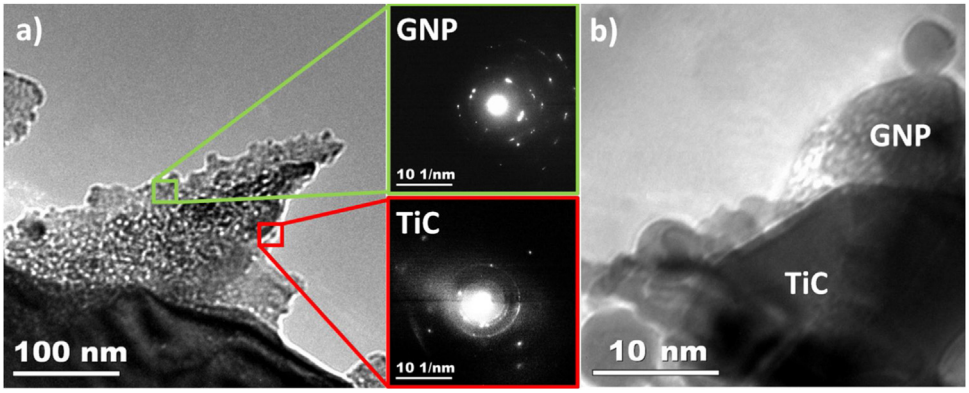

Fig. 7 – TEM image of GNPs coated with TiC and associated selected area diffraction pattern from GNPs and TiC nanoparticles.

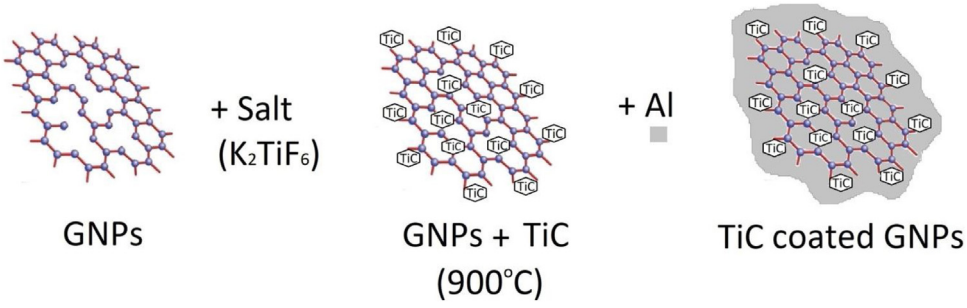

Fig. 8 – Model representing the titanium carbide coating on GNPs.

the carbonaceous substrate, as reported by Wong et al. [51]. TiC has a tendency to form under the influence of temperature and availability of active carbon at an atomic scale [52]. Fig. 7b shows high resolution TEM images with TiC nano particle and GNPs. The distinct morphology of TiC embedded in GNPs can be seen as marked on the figure.

3.6. *Mechanism*

The formation of TiC is an exothermic reaction [48]. An increase in temperature promotes the formation of localised nucleation of TiC on the surface of GNPs. The preferable sites are surface imperfections like unbounded carbon atoms, voids or defects in the graphitic structure of GNPs. Near the melting temperature of aluminium, the formation of TiC_2 starts [42]. Moreover, in the presence of $KAlF_4$, Al_2O_3 dissolves earlier, which is present on the surface of aluminium. At the melting temperature of aluminium, Al_3Ti starts forming, which was verified in XRD (Fig. 4) and also presented in Eqs. (2) and (4). In the presence of GNPs, Al_3Ti is converted into TiC. The conversion of Al_3Ti continues until the availability of available carbon cites on the sole source added in the mixture, i.e. GNPs (10). The molten aluminium was therefore readily available to coat the in situ TiC formed on the surface of GNPs. An illustrative model is presented in Fig. 8. The EDS spectrum in Fig. 3b confirms the fact that the GNPs have titanium wetted with aluminium on their surface. The molten aluminium also retains the elemental titanium to adequately react with available GNPs.

4. Summary and conclusions

In the present investigation, GNPs are heated at 900 °C in the presence of aluminium and potassium hexafluorotitanate salt. The ratio of titanium-to-carbon of 5:1, used in argon atmosphere, resulted in the formation of TiC coated on GNPs. An effort to address the negligible wetting of GNPs with aluminium, is carried out by coating in situ TiC. Following conclusions can be drawn from the study;

- EDS indicated the presence of elemental titanium and aluminium on the surface of GNPs, while XRD confirmed the formation of TiC.
- Thermal characterization revealed the mechanism of formation of TiC from precursor salt in aluminium melt. DTA helped in understanding the reaction kinetics and identification of the reaction products in a sequential manner.
- TGA/DSC results complemented the discussion regarding the salt decomposition and explanation of the in situ formation of TiC.
- TEM analysis confirmed the presence of TiC on GNPs. An illustrative model is presented to develop a comprehension regarding the mechanism of TiC formation on GNPs.

The results of the present investigation can provide a possibility to improve the wettability of GNPs in aluminium. The addition of hybrid nano reinforcements in aluminium would pave the path to overcome the clustering and agglomeration problems of GNPs in aluminium.

Conflict of interest

The authors declare no conflicts of interest.

Acknowledgments

The authors acknowledge the financial support of the Higher Education Commission of Pakistan (Grant No. 213-53249-2EG2-102) provided under Ph.D. indigenous fellowship; Phase-II Batch-II and to Norwegian University of Science and Technology (NTNU), Norway.

REFERENCES

[1] Khan M, Zulfaqar M, Ali F, Subhani T. Microstructural and mechanical characterization of hybrid aluminum matrix composite containing boron carbide and Al-Cu-Fe quasicrystals. Met Mater Int 2017;23(4):813–22.
[2] Khan M, Zulfaqar M, Ali F, Subhani T. Hybrid aluminium matrix composites containing boron carbide and quasicrystals: manufacturing and characterisation. Mater Sci Technol 2017;33(16):1955–63.
[3] Khan M, Rehman A, Aziz T, Shahzad M, Naveed K, Subhani T. Effect of inter-cavity spacing in friction stir processed Al 5083 composites containing carbon nanotubes and boron carbide particles. J Mater Process Technol 2018;253:72–85.
[4] Khan M, Syed WH, Akhtar S, Aune RE. Friction stir processing (FSP) of multiwall carbon nanotubes and boron carbide reinforced aluminum alloy (Al 5083) composites. Cham: Springer International Publishing; 2019.
[5] Khan M, Amjad M, Khan A, Ud-Din R, Ahmad I, Subhani T. Microstructural evolution, mechanical profile, and fracture morphology of aluminum matrix composites containing graphene nanoplatelets. J Mater Res 2017:1–12.
[6] Khan M, Rehman A, Aziz T, Naveed K, Ahmad I, Subhani T. Cold formability of friction stir processed aluminum composites containing carbon nanotubes and boron carbide particles. Mater Sci Eng A 2017;696:552–7.
[7] Wang J, Li Z, Fan G, Pan H, Chen Z, Zhang D. Reinforcement with graphene nanosheets in aluminum matrix composites. Scr Mater 2012;66(8):594–7.
[8] Balandin AA. Superior thermal conductivity of single-layer graphene. Nano Lett 2008;8(3):902–7.
[9] Huang X, Qi X, Boey F, Zhang H. Graphene-based composites. Chem Soc Rev 2012;41(2):666–86.
[10] Alam SN, Kumar L. Mechanical properties of aluminium based metal matrix composites reinforced with graphite nanoplatelets. Mater Sci Eng A 2016;667:16–32.
[12] Hu Q, Wang X-t, Chen H, Wang Z-f. Synthesis of Ni/graphene sheets by an electroless Ni-plating method. New Carbon Mater 2012;27(1):35–41.
[13] Liu C, Wang K, Luo S, Tang Y, Chen L. Direct electrodeposition of graphene enabling the one-step synthesis of graphene–metal nanocomposite films. Small 2011;7(9):1203–6.
[14] Li S, Su Y, Ouyang Q, Zhang D. In-situ carbon nanotube-covered silicon carbide particle reinforced aluminum matrix composites fabricated by powder metallurgy. Mater Lett 2016;167:118–21.
[15] Lekatou A, et al. Aluminium reinforced by WC and TiC nanoparticles (ex-situ) and aluminide particles (in-situ): microstructure, wear and corrosion behaviour. Mater Des 2015;65:1121–35.
[16] Liu G, et al. In-situ synthesis of graphene decorated with nickel nanoparticles for fabricating reinforced 6061Al matrix composites. Mater Sci Eng A 2017;699 Supplement C: 185–93.
[17] Liu X, et al. In-situ synthesis of graphene nanosheets coated copper for preparing reinforced aluminum matrix composites. Mater Sci Eng A 2018;709 Supplement C:65–71.
[18] Rana D, Mandal BM, Bhattacharyya SN. Analogue calorimetric studies of blends of poly(vinyl ester)s and polyacrylates. Macromolecules 1996;29(5):1579–83.
[19] Rana D, Mandal BM, Bhattacharyya SN. Analogue calorimetry of polymer blends: poly(styrene-co-acrylonitrile) and poly(phenyl acrylate) or poly(vinyl benzoate). Polymer 1996;37(12):2439–43.
[20] Rana D, Mandal BM, Bhattacharyya SN. Miscibility and phase diagrams of poly(phenyl acrylate) and poly(styrene-co-acrylonitrile) blends. Polymer 1993;34(7):1454–9.
[21] Kornilov II, Pylaeva EN, Volkova MA. Phase diagram of the binary system titanium-aluminum. Bull Acad Sci Ussr Div Chem Sci 1956;5(7):787–95.
[22] Qiu C, Metselaar R. Solubility of carbon in liquid Al and stability of Al4C3. J Alloys Compd 1994;216(1):55–60.
[23] Kevorkijan VM. Aluminum composites for automotive applications: a global perspective. JOM 1999;51(11):54–8.
[24] Koli DK, Agnihotri G, Purohit R. Advanced aluminium matrix composites: the critical need of automotive and aerospace engineering fields. Mater Today Proc 2015;2(4–5):3032–41.
[25] Tjong SC. Recent progress in the development and properties of novel metal matrix nanocomposites reinforced with carbon nanotubes and graphene nanosheets. Mater Sci Eng R Rep 2013;74(10):281–350.
[26] Yoo SJ, Kim WJ. Strength enhancement by shear-flow assisted dispersion of carbon nanotubes in aluminum matrix composite. Mater Sci Eng A 2013;570:102–5.
[27] Bauri R. Optimization of process parameters for friction stir processing (FSP) of Al–TiC in situ composite. Bull Mater Sci 2014;37(3):571–8.
[28] Thakur SK, Srivatsan TS, Gupta M. Synthesis and mechanical behavior of carbon nanotube–magnesium composites hybridized with nanoparticles of alumina. Mater Sci Eng A 2007;466(1):32–7.
[29] Kim WJ, Yu YJ. The effect of the addition of multiwalled carbon nanotubes on the uniform distribution of TiC nanoparticles in aluminum nanocomposites. Scr Mater 2014;72-73:25–8.
[30] Thakur SK, Tun KS, Gupta M. Enhancing uniform, nonuniform, and total failure strain of aluminum by using SiC at Nanolength Scale. J Eng Mater Technol 2010;132(4), 041002-041002-6.
[31] Baumli P, Sytchev J, Kaptay G. Perfect wettability of carbon by liquid aluminum achieved by a multifunctional flux. J Mater Sci 2010;45(19):5177–90.
[32] Mansoor M, Shahid, Muhammad. A facile one-step method of coating aluminum on multiwall carbon nanotubes. J Alloys Compd 2015.
[33] Li X, et al. Preparation of a titanium carbide coating on carbon fibre using a molten salt method. Carbon 2008;46(2):305–9.
[34] Rodriguez JL, et al. Novel system (K2TiF6-N2-Ti) to synthesize rod-like TiN nanopowders. Part Sci Technol 2016;34(3):324–31.

[35] Khan M, Ud Din R, Wadood A, Syed WH, Akhtar S, Aune RE. Effect of graphene nanoplatelets on the physical and mechanical properties of Al6061 in fabricated and T6 thermal conditions. J Alloys Compd 2019;790:1076–91.
[36] Birol Y. In situ synthesis of Al–TiCp composites by reacting K2TiF6 and particulate graphite in molten aluminium. J Alloys Compd 2008;454(1):110–7.
[37] Ahmad I, et al. Toughening mechanisms and mechanical properties of graphene nanosheet-reinforced alumina. Mater Des 2015;88:1234–43.
[38] Lü L, Lai MO, Yeo JL. In situ synthesis of TiC composite for structural application. Compos Struct 1999;47(1):613–8.
[39] Wang C-A, Zhou A, Qi L, Huang Y. Quantitative phase analysis in the Ti–Al–C ternary system by X-ray diffraction. Powder Diffr 2012;20(3):218–23.
[40] Zaykov YP, Isakov AV, Zakiryanova ID, Reznitskikh OG, Chemezov OV, Redkin AA. Interaction between SiO2 and a KF–KCl–K2SiF6 melt. J Phys Chem B 2014;118(6):1584–8.
[41] Batalu D, Cosmeleata G, Aloman A. Critical analysis of the Ti-Al phase diagrams. UPB Sci. Bull., Series B 2006;68(4):77–90.
[42] Birol Y. Analysis of the response to thermal exposure of Al/K2TiF6 powder blends. J Alloys Compd 2009;478(1–2):265–8.
[43] Prasad KVS, Murty BS, Pramanik P, Mukunda PG, Chakraborty M. Reaction of fluoride salts with aluminium. Mater Sci Technol 1996;12(9):766–70.
[44] Deng CF, Zhang XX, Wang DZ, Ma YX. Calorimetric study of carbon nanotubes and aluminum. Mater Lett 2007;61(14–15):3221–3.
[45] Feng Y-b, Yang B, Dai Y-n. Thermodynamics on formation of C, Al4C3 and Al2O3 in AlCl disproportionation process in vacuum to produce aluminum. Trans Nonferrous Met Soc China 2014;24(10):3366–71.
[46] Fan T, Yang G, Zhang D. Thermodynamic effect of alloying addition on in-situ reinforced TiB2/Al composites. Metall Mater Trans A 2005;36(1):225–33.
[47] Baklanova NI, Zaitsev BN, Titov AT, Zima TM. The chemistry, morphology, topography of titanium carbide modified carbon fibers. Carbon 2008;46(2):261–71.
[48] Dikici B, Gavgali M, Bedir F. Synthesis of in situ TiC nanoparticles in liquid aluminum: the effect of sintering temperature. J Compos Mater 2011;45(8):895–900.
[49] Sharma A, Sohn H-R, Jung JP. Effect of graphene nanoplatelets on wetting, microstructure, and tensile characteristics of Sn-3.0Ag-0.5Cu (SAC) alloy. Metall Mater Trans A 2016;47(1):494–503.
[50] Voevodin A, Prasad S, Zabinski J. Nanocrystalline carbide/amorphous carbon composites. J Appl Phys 1997;82:855–8.
[51] Wong EW, Maynor BW, Burns LD, Lieber CM. Growth of metal carbide nanotubes and nanorods. Chem Mater 1996;8(8):2041–6.
[52] Himbeault DD, Varin RA, Piekarski K. Tensile properties of titanium carbide coated carbon fibre — aluminum alloy composites. Composites 1989;20(5):471–7.